Understanding Dispersion Compensation of the THz Communication Channels in the Atmosphere

Mahboubeh Mandehgar and Daniel R. Grischkowsky, *Fellow, IEEE*

***Abstract*— We demonstrate that dispersive compensation can be achieved for THz communication channels within the atmospheric THz windows. However, THz pulse broadening cannot be eliminated due to the bandwidth reduction of the propagating THz pulse due to the frequency-dependent absorption of the channels.**

***Index Terms*— THz-TDS, THz communications, dispersion compensation.**

THERE ARE many applications for future high bit-rate THz links in the atmosphere, as described in the review articles [1]–[5], for which the absorption is considered to be constant across the bandwidth of the link and the dispersion of the refractivity is neglected. An important demonstration of a custom built NTT prototype wireless system, was the 800 m line-of-sight wireless transmission of live television broadcast coverage of the Beijing 2008 Olympics. The transmitted 10 mW, 10.3 Gb/s bit stream at 120 GHz, had simple amplitude shift keying, and a bit error rate of 10^{-12} [6].

Many other demonstrations have been reported that focus on modern THz communication technology, for example, a 2.5 Gbit/s error-free link at 625 GHz for several meters [7], a 25 Gbit/s MMIC-based link at 220 GHz for 10 m [8], and a 24 Gbit/s link at 300 GHz for 0.5 m [9]. Most recently, a 20 m direct digital link at 237.5 GHz with a bit rate of 100 Gb/s has been reported [10]. Also, a multi-channel 40 Gb/s link at 200 GHz for 2 cm has been reported [11].

These applications and the associated technology of transmitters, receivers, and interfacing to the optical fiber backbone are all dependent on the physical characteristics of the THz windows of transparency in the atmosphere, which define 7 THz communication channels up to 1000 GHz.

Consequently, it is important to demonstrate the fundamental limits of these channels [12]–[14], on which feasibility of many proposed applications will be based. These channels with minimum loss and relatively low group velocity and higher order dispersion were chosen to optimize their performance to transmit digital data, without regard for frequency band boundaries and bandwidth allocations. The properties of these channels should stimulate field testing and development, and serve as a guide to future frequency allocations.

Recent studies, based on the physical properties of these channels [12]–[15], presented experimental and theoretical characterizations of long and short-length, high bit-rate links for the seven THz communication channels in the atmosphere below 1 THz [12]–[14]. These studies involved summations over the HITRAN database [16]. Although these studies focused on short THz pulse transmission through the atmosphere, the characterizations are valid for any form of modulation.

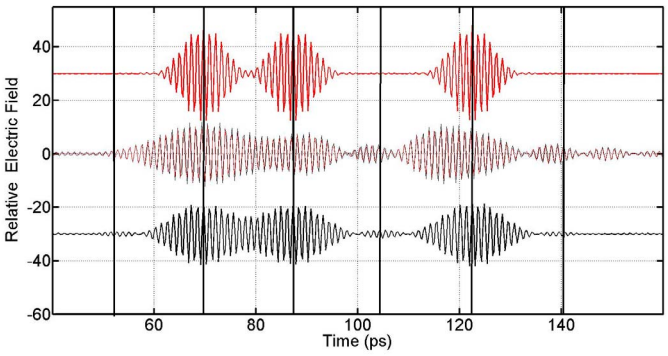

Fig. 1. Comparison of experiment and theory for **Channel 7**, 852 GHz, 56.8 Gb/s, (15 cycles), 108 GHz BW, for 137-m path propagation with RH 65% (11.2 g/m^3) and 21 °C [13]. The black vertical lines mark the centers of the bit slots. Upper (red) input pulses, divided by 4 for better display. Middle (red) simulated output pulses, together with overlapping middle (black) measured output pulses [13]. New lower (black) compensated IFFT output pulses, showing non-return to zero bit resolution for the receiver.

Here, using a complete theoretical approach for the absorption and dispersion of water vapor, which is based on the most accurate characterization to date [13]–[15], we show the potential to increase the previous bit-rate distance products [12]–[14], by dispersion compensation. However, we also show that the frequency dependent absorption within the channels significantly reduces the bandwidth of the transmitted signal. This reduction also broadens the THz data pulses, and consequently dispersion compensation cannot eliminate all of the observed pulse broadening with propagation. These studies focus on the physical properties of the channels and do not include system engineering aspects. The future technical approaches will need to be compatible with the channel properties.

Figure 1 shows the recently studied input THz bit sequence (011010) for the 852 GHz channel and the measured and calculated output THz bit sequence [13]. The dispersion compensated bit sequence is shown as the bottom sequence. Clearly, the transmitted bit sequence has been improved by the compensation, but the clarity of the input sequence has not been obtained, because of the bandwidth narrowing due to absorption.

Manuscript received June 22, 2015; revised July 15, 2015; accepted August 7, 2015. Date of publication August 11, 2015; date of current version September 30, 2015.

The authors are with the School of Electrical and Computer Engineering, Oklahoma State University, Stillwater, OK 74078 USA (e-mail: m.mandehgar@okstate.edu; daniel.grischkowsky@okstate.edu).

Color versions of one or more of the figures in this letter are available online at http://ieeexplore.ieee.org.

Digital Object Identifier 10.1109/LPT.2015.2466559

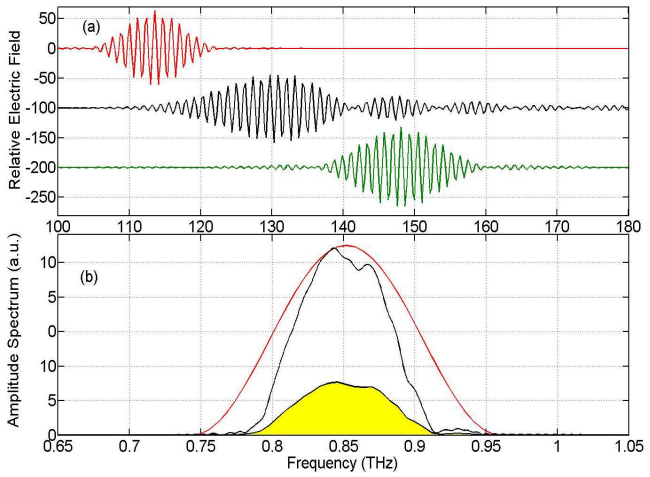

Fig. 2. (a). Upper (red) input pulse, middle (black) transmitted output pulse and lower (green) IFFT dispersion compensated output pulse, both multiplied by 3.5. Pulses are shown from 100 to 180 ps. (b). Input amplitude spectrum upper (red) line and output amplitude spectrum lowest (black) high-lighted line, also shown with multiplication as the middle (black) line.

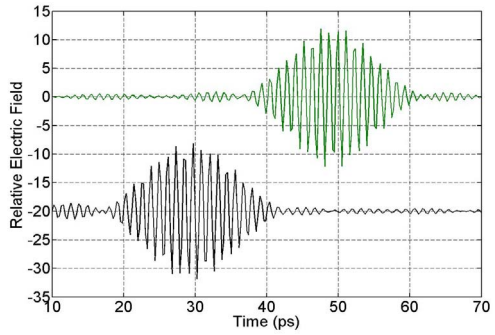

Fig. 3. Upper (green) IFFT dispersion compensated output pulse. Lower (black) output pulse with the Φ_C dispersion compensation of A_2 and A_3.

For the experimental conditions of Fig. 1, Fig. 2 shows a single THz input pulse, the transmitted output pulse, a completely dispersion compensated output pulse, and the corresponding amplitude spectra. The output spectrum is shown with reduced amplitude due to the frequency-dependent absorption of the channel. The FWHM bandwidth of the output spectrum is 76 GHz compared to the input bandwidth of 108 GHz. This reduction in bandwidth increases the width of the completely dispersion compensated output pulse shown in Fig. 2(a), compared to the input pulse. The compensated output pulse is simply obtained by the Inverse Fast Fourier Transform (IFFT) of the output amplitude spectrum. The increase in the transform limited output pulsewidth is inversely proportional to the reduced bandwidth of the output spectrum.

It is a mathematical fact, that the IFFT of the amplitude spectrum of an arbitrary phase modulated pulse will give the transform limited, dispersion compensated, pulseshape. The technical challenge is whether this can be achieved with physically realizable linear filters or phase modulators.

Figure 3 compares the IFFT dispersion compensated output pulse with the Φ_c (A_2 and A_3), dispersion compensated pulse, which shows excellent compensation. The small GVD β_2 correction is proportional to the squared frequency-difference from the carrier. To achieve the excellent dispersion compensation shown in Fig. 3, we needed to include the dominating contribution from the next higher order term, β_3 proportional to the cubed frequency-difference.

When the electric field of the input THz pulse, E(0, ω), (expressed in the frequency domain) passes through the dispersive atmosphere, the phase changes due to the resonance lines of water vapor. The output complex spectrum E (z, ω), is given by the product of the input field with the phase function and the attenuation, as

$$E(z,\omega) = E(0,\omega)\cdot e^{i\Delta k(\omega)z}\cdot e^{-\alpha(\omega)z/2}. \quad (1)$$

$$\Phi(\omega) = \Delta k(\omega)\, z = \beta(\omega)\, z \quad (2)$$

$\beta(\omega)$ is the precisely calculated propagation vector [13]–[16], $\alpha(\omega)$ is the attenuation coefficient, and z is the propagation distance. For communication channels, $\beta(\omega)$ is approximated by a Taylor series with respect to the carrier (center) angular frequency ω_o of the pulse. From [13, eq. (2)], the Taylor series expression for the approximate $\beta_A(\omega)$ is given by

$$\beta A(\omega) = \beta(\omega 0) + \beta_1(\Delta\omega) + \frac{1}{2}\beta_2(\Delta\omega)^2 + \frac{1}{3!}\beta_3(\Delta\omega)^3 \quad (3)$$

for which $\Delta\omega = (\omega - \omega_o)$, and β_1 , β_2 and β_3 are the first, second and third derivatives of $\beta(\omega)$ with respect to ω, respectively. β_2 is the group velocity dispersion.

Our general approach is to calculate the frequency dependent phase $\Phi(\omega, z)$ of the propagated pulse, due to the refractivity (n(ω) – 1), where n(ω) is the frequency dependent index of refraction of the atmosphere. For this case, we remove the strong linear phase ramp as follows: $\Phi(\omega, z) = \beta(\omega)z = (\omega/c)\,(n(\omega) - n(0) - 2)z$, for which $(n(0) - 1) = (61.06 \times 10^{-6})$ for a water vapor density of 10 g/m^3 [15], which is increased to 68.4×10^{-6}, for a density of 11.2g/m^3.

For the numerical calculations, it is helpful to rewrite the approximate phase equation $\Phi_A(\omega,z) = \beta_A(\omega)z$, in the form

$$\Phi_A = \Phi_0 + A_1\Delta\omega + A_2\Delta\omega^2 + A_3\Delta\omega^3. \quad (4a)$$

$$\Phi_C = A_2\Delta\omega^2 + A_3\Delta\omega^3. \quad (4b)$$

The THz bit pulse reshaping and broadening are due to the A_2 and the A_3 terms, while $\Phi_0 = \beta(\omega_0)z$ and A_1 determine the speed of undistorted pulse propagation. The compensating phase modulation is given by Φ_C. Specifying this dependence, the curve fitting tool of MATLAB was used to optimize the 3-A coefficients to fit the calculated phase Φ_A over the bandwidth. This phase comparison is very sensitive to the resonant line structure within and near the THz communication channel under study, and best dispersion compensation may require center frequency adjustment and bandwidth reduction. We have found that best performance is obtained, when the phase fitting process to determine the 3-A parameters is done within the output FWHM amplitude spectral range. The resulting A parameters are then used to calculate $\Phi_A(\omega, z)$ over the entire spectrum.

Figure 4a shows the complete phase calculation (black line) of $\beta(\omega)z$ without the constant (zero frequency) refractivity term [13]–[15], compared to the (almost identical) 3-A parameter fit of Φ_A (purple line) with $(\omega_o/2\pi) = 852$ GHz, marked by the vertical line. Figure 4b shows the phase modulation Φ_C, which is responsible for the pulse reshaping and broadening, given by the two curves of Fig. 4a minus

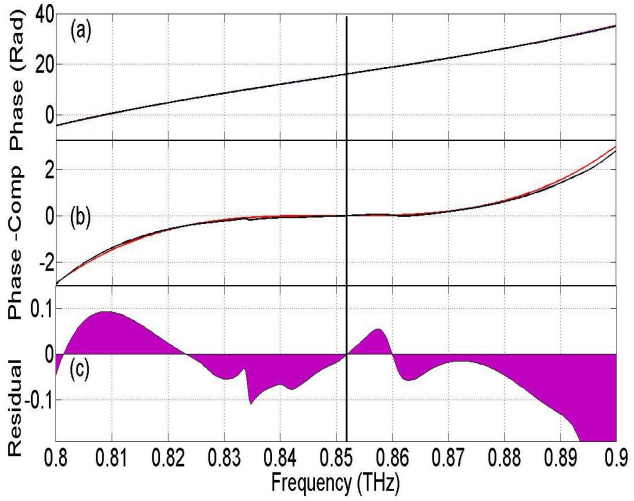

Fig. 4. All curves are shown in radians. (a). Calculated phase angle Φ for the conditions of Fig. 1 [13], (black line) and the 3-A parameter Φ_A result of Eq. (4a) (purple line). (b). Compensating phase modulation for the complete theory (black line) and for (purple line) Φ_C. (c). The overlapping residual plots between the two (a) and the two (b) curves.

the curve $(\Phi_0 + A_1\Delta\omega)$. The black curve is for the complete theory and the purple curve is the optimized compensating phase modulation Φ_C. The fit is so good, that the two lines can barely be resolved. The asymmetry of the phase modulation, with respect to 852 GHz shows that the strong antisymmetric β_3 component dominates the smaller symmetric GVD β_2 component. At 900 GHz the $A_3\Delta\omega^3$ term is 7.4 times larger than the $A_2\Delta\omega^2$ term.

The difference between the two plots (residuals) shown in Fig. 4c, indicates a fitting precision of the order of ± 0.05 rad. The strong frequency dependence of the residual plot is due to several very weak water lines that are in the HITRAN comprehensive data base for water vapor lines [16], used for the complete theory. Here, dispersion compensation is performed by multiplying the complex output spectrum by $\exp(-i\Phi_c)$. The lower compensated pulse in Fig. 3 shows the effectiveness of this approach.

Figure 5 shows dispersion compensation for the lower frequency Channel 3 at 255 GHz [13], [14]. The transmitted pulse sequence (middle trace) can no longer be resolved after passage through 4 km of the atmosphere with a water vapor density of 10 g/m^3. However, when this calculated transmitted pulse sequence is completely dispersion compensated by IFFT, the transmitted pulse sequence changes to the bottom trace with resolution of the non-return to zero bit sequence for the receiver. For the excellent dispersion compensation of Φ_C, the restored pulse sequence is almost identical for the IFFT output pulse and the Φ_C, 2-A parameter fit pulse.

Figure 6 shows a single input pulse and the calculated, propagated output pulse for the same conditions as Fig. 5. The input pulse is smoothly broadened by the 4-km propagation into the transmitted output pulse with a linear frequency chirp to higher frequencies. The extensive pulse broadening shows the need for dispersion compensation.

The corresponding spectra of Fig. 6 are shown in Fig. 7a. The transmitted spectrum is very smooth with no complicated features due to the 183 GHz resonance line of water vapor [13]–[16]. The FWHM of the attenuated output spectrum is 66 GHz, compared to 80 GHz for the input.

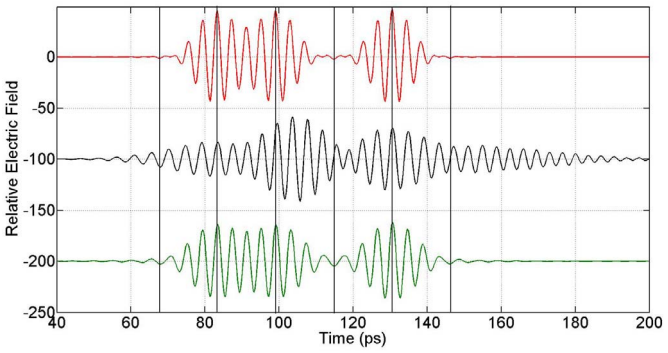

Fig. 5. Calculated digital pulse transmission for **Channel 3**, 255 GHz, 64 Gb/s, (4 cycles), 80 GHz BW, for 4-km path propagation with RH 58% (10.0 g/m^3) and 20 °C [13].The black vertical lines mark the centers of the bit slots. Upper (red) input pulses. Middle (black) calculated output pulses, multiplied by 6 for better comparison. Lower (green) dispersion compensated output pulses, using Φ_C.

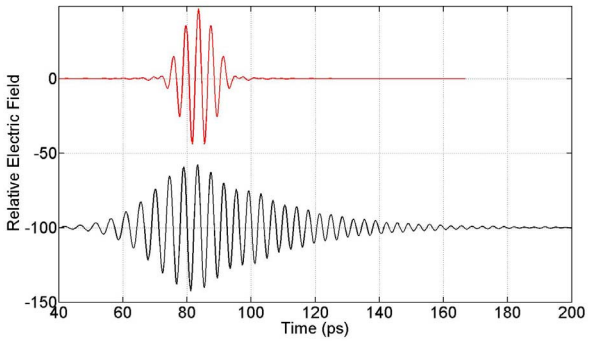

Fig. 6. Calculated digital pulse transmission for **Channel 3**, 255 GHz, 80 GHz BW, for 4-km path propagation with RH 58% (10.0 g/m^3) and 20 °C [13].The red upper input pulse and the black lower transmitted pulse multiplied by 6 for better display of the extensive broadening and amplitude reduction due to absorption.

The amplitude ratio of the output to input spectra at 255 GHz is 0.156, giving a power absorption of 16.1 dB. The dispersion compensated. IFFT output pulse is presented in Fig. 7b. The 2-A parameter Φ_C. compensated pulse of Fig. 7c is remarkably similar to the IFFT output pulse of Fig. 7b.

Figure 8a shows the complete theory calculated phase $\Phi(\omega,z)$ for the 4-km path propagation with RH 58% (10.0 g/m^3) and 20 °C [14], compared to the (almost identical) 3-A parameter fit for $\Phi_A(\omega,z)$ of Eq. (2a), with $(\omega_o/2\pi) = 255$ GHz, marked by the vertical line. Figure 8b shows the two curves of 8a minus the curve for $(\Phi_0 + A_1\Delta\omega)$. The black curve is for the complete theory and the purple curve is the optimized compensating phase modulation Φ_C. Again, the fit is so good that the two lines can barely be resolved. The approximate symmetry of the phase with respect to 255 GHz shows mainly GVD β_2 dispersion, with a smaller β_3 contribution, in contrast to the asymmetry of Fig. 4b. At 295 GHz the symmetric $A_2\Delta\omega^2$ term is 4.3 times larger than the antisymmetric $A_3\Delta\omega^3$ term. Figure 8c shows the small phase differences of the order of 0.02 radians between the two curves of Fig. 8a, which increase to above 0.05 radians above 295 GHz. Again, the strong frequency dependence of the residual plot is due to several very weak water lines in the complete HITRAN database [16].

In summary, we have demonstrated that dispersion compensation can be achieved for the THz communication channels within the atmospheric THz windows. However, the THz

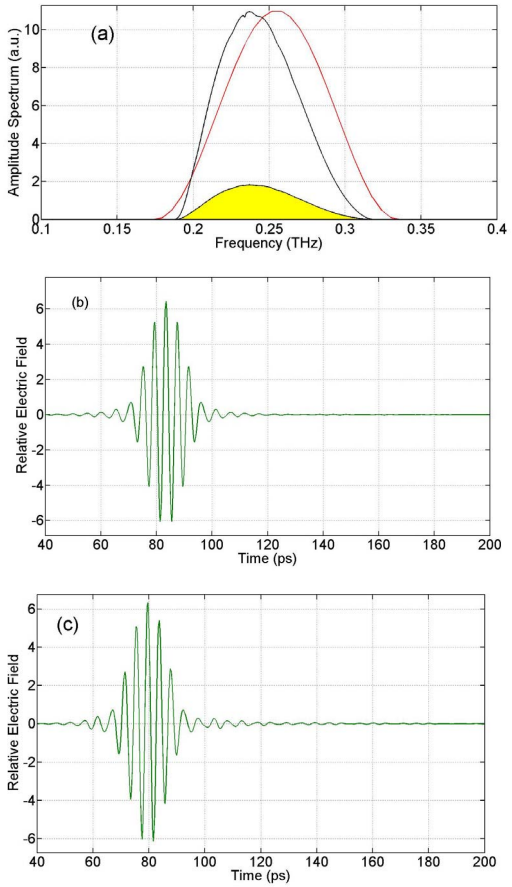

Fig. 7. (a). Amplitude spectrum (red line) of 255 GHz input pulse of Fig. 6. Amplitude spectrum (lower black high-lighted line) of the calculated output pulse of Fig. 6. Middle black line is the output amplitude spectrum multiplied by 6 to better show linewidth reduction due to absorption. Input FWHM BW 80 GHz. Output BW 66 GHz. (b). Dispersion compensated IFFT output pulse. (c) Dispersion compensated output pulse, using Φ_C.

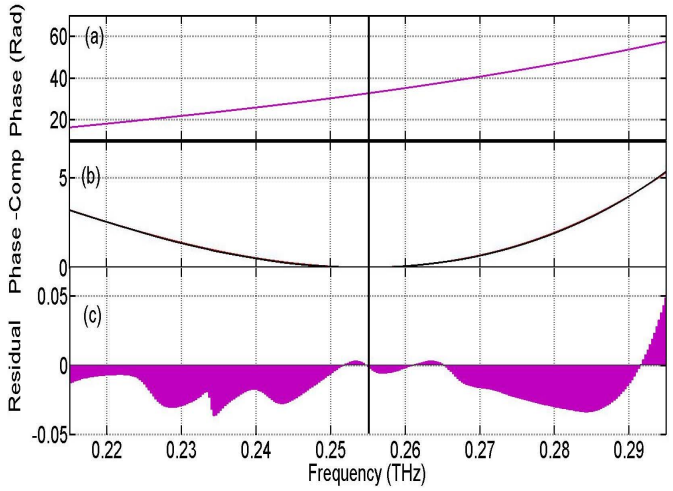

Fig. 8. All curves are shown in radians. (a). Calculated phase angle Φ for the conditions of Fig. 5 (black line) and the 3-A parameter Φ_A result of Eq. (4a) (purple line). (b). Compensating phase modulation for the complete theory (black line) and for (purple line) Φ_C. (c). The overlapping residual plots between the two (a) curves and the two (b) curves.

pulse broadening cannot be eliminated due to the bandwidth reduction of the propagating THz pulse due to the frequency dependent absorption of the channels.

We have demonstrated that it is possible to achieve essentially complete dispersion compensation in the two atmospheric THz communication channels 3 at 255 GHz and 7 at 852 GHz. The dispersion compensation over the FWHM amplitude frequency bandwidth varied smoothly between 0 and 5, radians and ± 3 radians, for channels 3 and 7, respectively. Channel 3 was well fit by the standard GVD β_2 term together with a smaller next higher order β_3 term. Channel 7 was well fit by the higher order β_3 term together with a much smaller β_2 term. With optimal choice of center frequency and bandwidth, this approach could be applied to the other five THz communication channels below 1 THz [13], [14]. For application to future operating THz links, such compensation would have to be able to follow the changes of water vapor density of the atmosphere, by proportional changes of the amplitude of the compensating phase modulation.

REFERENCES

[1] R. Piesiewicz *et al.*, "Short-range ultra-broadband terahertz communications: Concepts and perspectives," *IEEE Antennas Propag. Mag.*, vol. 49, no. 6, pp. 24–39, Dec. 2007.

[2] J. Wells, "Faster than fiber: The future of multi-Gb/s wireless," *IEEE Microw. Mag.*, vol. 10, no. 3, pp. 104–112, May 2009.

[3] J. Federici and L. Moeller, "Review of terahertz and subterahertz wireless communications," *J. Appl. Phys.*, vol. 107, no. 11, p. 111101, 2010.

[4] H.-J. Song and T. Nagatsuma, "Present and future of terahertz communications," *IEEE Trans. Terahertz Sci. Technol.*, vol. 1, no. 1, pp. 256–263, Sep. 2011.

[5] A. J. Seeds, H. Shams, M. J. Fice, and C. C. Renaud, "TeraHertz photonics for wireless communications," *J. Lightw. Technol.*, vol. 33, no. 3, pp. 579–587, Feb. 1, 2015.

[6] T. Kosugi, A. Hirata, T. Nagatsuma, and Y. Kado, "MM-wave long-range wireless systems," *IEEE Microw. Mag.*, vol. 10, no. 2, pp. 68–76, Apr. 2009.

[7] L. Moeller, J. Federici, and K. Su, "THz wireless communications: 2.5 Gb/s error-free transmission at 625 GHz using a narrow-bandwidth 1 mW THz source," in *Proc. 30th URSI General Assembly Sci. Symp. (URSI GASS)*, Istanbul, Turkey, 2011, pp. 1–4.

[8] I. Kallfass, J. Antes, D. Lopez-Diaz, S. Wagner, A. Tessmann, and A. Leuther, "Broadband active integrated circuits for terahertz communication," in *Proc. 18th Eur. Wireless Conf. Eur. Wireless (EW)*, 2012, pp. 1–5.

[9] H.-J. Song, K. Ajito, Y. Muramoto, A. Wakatsuki, T. Nagatsuma, and N. Kukutsu, "24 Gbit/s data transmission in 300 GHz band for future terahertz communications," *IET Electron. Lett.*, vol. 48, no. 15, pp. 953–954, 2012.

[10] S. Koenig *et al.*, "Wireless sub-THz communication system with high data rate," *Nature Photon.*, vol. 7, pp. 977–981, Oct. 2013.

[11] H. Shams, M. J. Fice, K. Balakier, C. C. Renaud, A. J. Seeds, and F. van Dijk, "Multichannel 200 GHz, 40 Gb/s wireless communication system using photonic signal generation," in *Proc. Int. Topical Meeting Microw. Photon., 9th Asia-Pacific Microw. Photon. Conf.*, Oct. 2014, pp. 366–369.

[12] M. Mandehgar, Y. Yang, and D. Grischkowsky, "Atmosphere characterization for simulation of the two optimal wireless terahertz digital communication links," *Opt. Lett.*, vol. 38, no. 17, pp. 3437–3440, 2013.

[13] M. Mandehgar, Y. Yang, and D. Grischkowsky, "Experimental confirmation and physical understanding of ultra-high bit rate impulse radio in the THz digital communication channels of the atmosphere," *J. Opt.*, vol. 16, no. 9, pp. 094004-1–094004-17, 2014.

[14] Y. Yang, M. Mandehgar, and D. Grischkowsky, "THz-TDS characterization of the digital communication channels of the atmosphere and the enabled applications," *J. Infr., Millim., Terahertz Waves*, vol. 36, no. 2, pp. 97–129, 2015.

[15] D. Grischkowsky, Y. Yang, and M. Mandehgar, "Zero-frequency refractivity of water vapor, comparison of Debye and van-Vleck Weisskopf theory," *Opt. Exp.*, vol. 21, no. 16, pp. 18899–18908, 2013.

[16] L. S. Rothman *et al.*, "The HITRAN 2012 Molecular Spectroscopic Database," *J. Quant. Spectrosc. Radiat. Transf.*, vol. 130, pp. 4–50, Nov. 2013.